Scientific Research Publishing

Advances in Materials Physics and Chemistry, 2022, 12, 106-123
https://www.scirp.org/journal/ampc
ISSN Online: 2162-5328
ISSN Print: 2162-531X

Environmentally Friendly Bifunctional Catalyst for ORR and OER from Coconut Shell Particles

Maryam Jahan[1*], Foster Feni[2]

[1]Department of Biological Sciences and Chemistry, Southern University and A & M College, Baton Rouge, LA, USA
[2]Mechanical Engineering Department, Southern University and A & M College, Baton Rouge, LA, USA
Email: *maryam_jahan@subr.edu

How to cite this paper: Jahan, M. and Feni, F. (2022) Environmentally Friendly Bifunctional Catalyst for ORR and OER from Coconut Shell Particles. *Advances in Materials Physics and Chemistry*, **12**, 106-123.
https://doi.org/10.4236/ampc.2022.125008

Received: April 19, 2022
Accepted: May 28, 2022
Published: May 31, 2022

Abstract

Catalyst for oxygen evolution reaction (OER) and oxygen reduction reaction (ORR) is at the heart of key renewable energy technologies such as water splitting and rechargeable batteries. But developing a low-cost oxygen electrode catalyst with high activity at low overpotential remains a great challenge. Coconut shells can be utilized as suitable raw material to produce activated carbon for enhanced adsorption capacity, bulk density, and hardness to be used as regenerative fuel cells running ORR and OER. The present work is designed to obtain an alternative to noble metal-based catalysts by synthesizing electroactive N-doped porous carbon from coconut shells; the use of biodegradable raw material through a single-step activation followed by nitrogen doping provides a more economical and environmentally friendly route to produce green catalysts for fuel cell applications. In valorization of biomass for the development of novel catalytic materials, our aim is also to reduce the use of hazardous chemicals. N-doped activated carbon shows promising bifunctional catalyst for ORR and OER as low-cost noble-metal-free and carbon-based oxygen catalysts.

Keywords

Bifunctional Catalyst, Oxygen Reduction Reaction, Oxygen Evolution Reaction, Coconut Shells, Carbon-Based Oxygen Catalyst

1. Introduction

The oxygen reduction reaction (ORR) and oxygen evolution reaction (OER) are very important in several renewable energy conversion and storage technologies, such as fuel cells [1], direct solar driven water splitting [2], hydrogen production from water electrolysis [3], rechargeable metal-air batteries [4], and regenerative fuel cells [5]. The slow activity of ORR on the cathode side is the impediment of

fuel cell application, while OER, a reverse reaction of ORR, is important in the efficiency of energy storage such as direct solar driven water splitting systems, Li-air batteries and regenerative fuel cells. Common ORR catalysts used are platinum and its alloy [6] while metal oxides/hydroxides of iridium and ruthenium have been mostly used as OER catalysts [7]. However, the OER/ORR is sluggish, even when facilitated by these catalysts. The main bottleneck of mass production of fuel cells is the limited resources and high cost of the platinum catalysts. Hence, it is challenging to design an efficient low-cost bifunctional OER and ORR catalysts used for rechargeable metal-air batteries and regenerative fuel cells.

Considering environmentally friendly catalysts, porous carbons with electroactive properties produced from natural resources and lignocellulosic biomass captured a lot of attention. N-doped carbon materials have been synthesized for example from bacterial cellulose [8] [9], cellulose nanocrystals [10], glucose and soy proteins [11], chitin [12] [13], chitosan [14] [15] [16] lignin [17], and plant biomass [18] [19]. The synthesis of multiple heteroatom-doped carbons has also been reported by direct pyrolysis of ginkgo leaves [20] and seaweeds [21].

Coconut shells as an important bioresource in tropical areas can be found in large quantities with high carbon content and low ash residues [22] [23]. The elemental composition showed that coconut shells contained higher content of carbon and low H/C and O/C ratio that is due to the large lignin content [24] [25] [26]. Compared to the other agricultural biomass, the density of the raw coconut shells is among the highest and the porosity is among the least [26]. This means that the morphology of the plant cells of the coconut shell is more compact due to the stronger cross-linking of the cellulose, hemicellulose, and lignin. As a result, the coconut shells can be utilized as suitable raw material to produce activated carbon for the adsorption capacity, bulk density, pore structure and hardness. The present work is designed to obtain an electroactive N-doped porous carbon via an economical and environmentally friendly process through single-step activation with nitric acid, followed by nitrogen doping using urea. In valorization of biomass for the development of novel catalytic materials, our aim is also to reduce the use of hazardous chemicals.

2. Experimental

2.1. Materials Synthesis

All chemicals purchased were of the purest grade and used as received from Sigma-Aldrich unless otherwise stated.

Coconuts were purchased from a local market (Walmart, USA) and their shells were grinded. 25 g of powdered coconut shell was chemically soaked overnight with 50 wt% HNO_3, followed by drying at 70˚C - 80˚C for 6 h. The carbonization was carried out under nitrogen flow at 550˚C for 2 h. The obtained carbon was washed with hot water and then immersed in 3 M HNO_3 overnight and finally filtered and dried at 105˚C. To enhance the interaction of urea with

the activated carbon surface, the sample was treated with 2 M HNO_3/1 M H_2SO_4 (1:1 v/v) at 120˚C for 2 h (functionalization treatment). For nitrogen doping of the activated carbon, a post-treatment was performed by dispersion in 1 M urea solution overnight. The resultant dispersion was filtered and dried, followed by pyrolysis at 900˚C for 2 h at 5˚C·min^{-1}. Figure 1 shows synthesis method of N-doped activated carbon and its usage for the electrochemical applications.

2.2. Characterization

The morphologies of the obtained samples were firstly characterized by using scanning electron microscopy (SEM) (JSM 6610LV, JEOL, Japan) operating at 15 KV. Kratos Axis 165 X-ray photoelectron spectroscope (XPS) was used to measure XPS spectra of the samples using Al Kα 1486.6 eV X-rays. High resolution spectra of C-1s, N-1s, O-1s were collected on the samples. During data acquisition runs, passing energy of 160 eV, current at 10 mA, and a time of 20 ms per step were used. Thermal Gravimetric Analysis (TGA) was performed using a thermogravimetry/differential Seiko analyzer TGA/DTA 6200 in a temperature range of 25˚C - 1000˚C at a heating rate of 10˚C·min^{-1} under air condition. Raman spectroscopy was carried out using a Renishaw in via Reflex Raman Microscope. Raman shifts within 150 cm^{-1} of the excitation frequency can be measured at excitation wavelengths of either 532 nm, 633 nm, or 785 nm, with a spectral resolution of 1 cm^{-1}. Fourier-transform infrared spectroscopy (FTIR) (Thermoscientific Nicolete iS-10) was carried out to characterize the functional chemical groups of the char. Also, X-ray diffraction (XRD) analysis was performed using a Mini Flex 600 benchtop machine (Regaku, Japan) with 2Θ scanning range from 5˚ to 90˚.

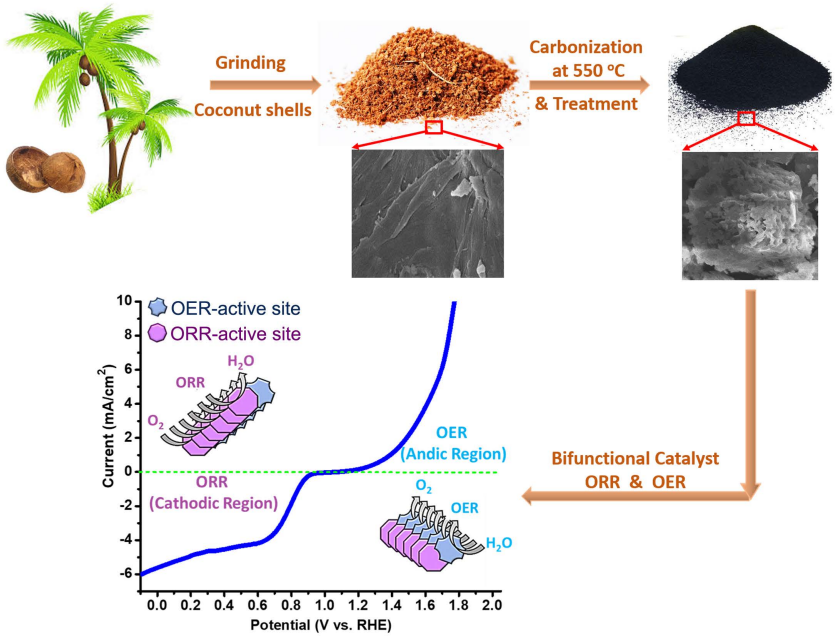

Figure 1. Schematic view of synthesis of N-doped activated carbon and usage for electrochemical measurement.

2.3. Electrochemical Measurements

All measurements were carried out at room temperature using a potentiostat (A-METEC) with a three-electrode electrochemical cell. We used an interchangeable glassy carbon (GC) disk electrode with a 5 mm diameter (area of 0.196 cm^2) as the working electrode, a platinum (Pt) wire as the counter electrode, and Hg/HgO (in saturated KOH solution) as the reference electrode. The GC disk was mechanically polished to achieve a mirror-like finish on the top surface of the electrode. Finally, the GC electrode was sonicated in ultrapure water, ethanol, and then again in ultrapure water and dried at room temperature before applying the catalyst ink. Linear sweep voltammetry (LSV) measurements were performed in O_2-saturated 0.1 M KOH solutions at a scan rate of 10 $mV \cdot s^{-1}$. RDE measurements were performed at rotation rates varying from 500 to 2500 rpm depending on the measurement, with the scan rate of 10 $mV \cdot s^{-1}$.

To prepare the catalyst ink for electrochemical measurements, 5 milligrams of the synthesized sample was mixed with the following solution: 1.25 mL of 3:2 Isopropanol/water solution, and 50 µl Nafion (5 wt%); this solution was sonicated for 1 h to achieve homogenous ink. Then a 20 µl drop of the catalyst ink was loaded on the polished surface of the glassy carbon electrode (GCE) and dried slowly at room temperature to achieve a uniform surface. Once the sample was completely dried, we estimated the amount of the sample delivered to the surface was 400 $\mu g/cm^2$. The sample was used in electrochemical measurements immediately after drying. Finally, Pt/C catalyst was used for comparisons and prepared exactly as the synthesized sample to achieve a similar loading of 400 $\mu g/cm^2$ of Pt/C (20 wt%).

3. Result and Discussion

3.1. Characterization and Heteroatom Doping

The surface morphology of the activated carbon was studied using scanning electron microscope (SEM), as shown in Figure 2. The raw coconut shell shows bulky morphology with a smooth surface, and no pores can be observed from Figure 2(A), however, smaller three-dimensional structures including pores were created upon doping with Nitrogen (Figure 2(B)). Lack of porosity of raw coconut shells is due to strong cross-linking of cellulose, hemicellulose, and

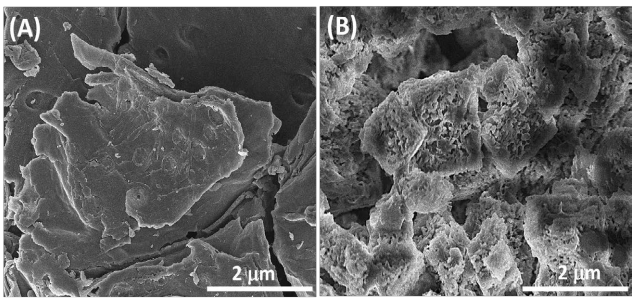

Figure 2. SEM image of (A) shows raw coconut shells and (B) is representative of our sample upon doping with Nitrogen.

lignin [26]. The presence of numerous voids allows the activation agent (herein urea) to freely access and disperse uniformly in coconut shells, resulting in the formation of porous materials [27]. The special structure of coconut biomass shortens the mass transport path and minimizes the diffusion resistance of target substances, resulting in significant improvement in properties.

XRD analysis was performed to identify the phase formed. XRD measurement was performed from an angle of 5˚ to 90˚ at a step rate of 0.2. **Figure 3(a)** shows XRD pattern obtained for raw coconut particles before carbonization and after N-doped. The predominant diffraction maxima observed for raw coconut are around 16.6˚, 22˚ and 34.6˚, which represents Cordierite ($Mg_2Al_4Si_5O_{18}$), Quartz (SiO_2), and moissanite (SiC), respectively [28], with quartz having the highest intensity. The diffraction maxima occurring at 2 theta of 27˚ and 44˚ represents silicate minerals and sodalities respectively [29]. The wide X-ray diffraction (XRD) pattern of N-doped Activated Carbon (**Figure 3(b)**) further confirms its amorphous nature. Two weak and broad diffraction maxima at around 23˚ and 43˚ were observed for this sample, which correspond to the (002) and (100) diffraction patterns of amorphous graphitic carbon [30]. Some diffraction maxima disappeared after N doping which is due to overlapping with (002) broad peak.

XPS spectra of N-doped activated carbon sample are shown in **Figure 4**. C1s binding energy (BE) can be seen in **Figure 4(A)**, indicating sp^2 C (284.7 eV), sp^3 C (284.9 eV), C-O/C-N (286.2 eV), and π excitation (290.7 eV). We can see O1s BE from the XPS spectra in **Figure 4(B)**; O-C (531.5 eV), O=C (532.4 eV), and O-C=O (534.1 eV) [31]. **Figure 4(C)** also shows the XPS spectra of functionalized graphene in N1s BE range. The XPS spectra have been fitted to get detailed chemical bonding information of the elements N and O with carbon. Nitrogen is observed in the sample confirming its incorporation into carbon structure. Generally, there are several nitrogen functional groups in nitrogen-functionalized carbon structure. These include pyridinic-N (BE = 396.1 eV),

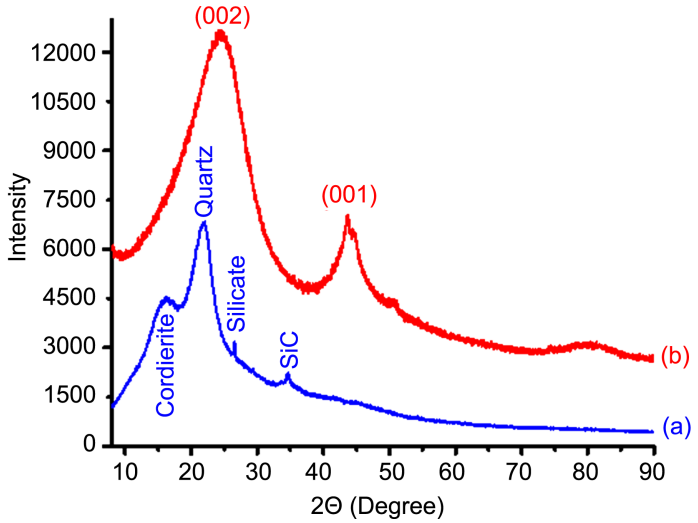

Figure 3. XRD diffraction pattern of (a) Raw coconut shell and (b) N-doped activated Carbon.

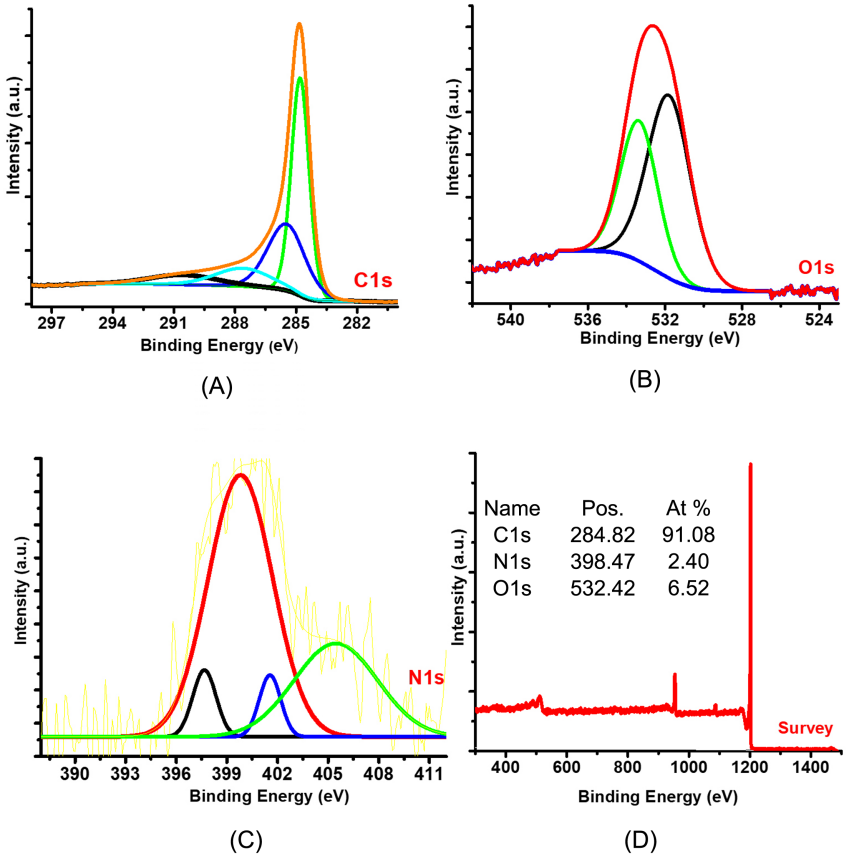

Figure 4. XPS spectra of N-doped activated Carbon. (A) C1s binding energy, (B) O1s binding energy, (C) N1s binding energy and (D) survey of the presence elements.

pyrrolic-N (BE = 400.2 eV), quaternary nitrogen (BE = 401.9 eV), and N-oxides of pyridinic-N (BE = 403.2 eV) [32] [33] [34].

The nitrogen functional groups are usually in the following molecular structures (chemical states) [32] [33] [34]: pyridinic-N refers to nitrogen atoms at the edge of graphene planes, each of them is bonded to two carbon atoms and donates one π-electron to the aromatic π-system; pyrrolic-N refers to nitrogen atoms that are bonded to two carbon atoms and contribute to the p system with two π-electrons; quaternary nitrogen is also called "graphitic nitrogen" or "substituted nitrogen", in which nitrogen atoms are incorporated into the graphene layer and replace carbon atoms within a graphene plane; N-oxides of pyridinic-N (pyridinic-(N^+ - O)) are bonded to two carbon atoms and one oxygen atom. **Figure 4(D)** shows the survey of the presence elements

Raman peak detected in **Figure 5** between 1339 and 1348 cm^{-1} can be assigned to D band characteristic of the disorder while the peak observed between 1586 and 1593 cm^{-1} can be attributed to the graphitic G band according to literature [35]. The D-band indicates the presence of defects in the graphitic materials due to bond-angle disorder, bond-length disorder, vacancies edge defects, etc. On the other hand, G-band is related to the stretching motion of the pairs of carbon sp^2 atoms while the broad peak in 2D-band indicates the number of layers formed [36].

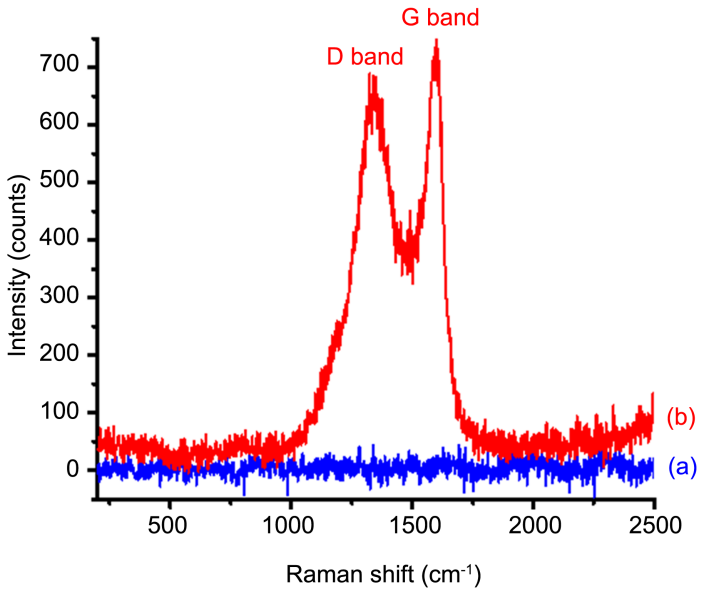

Figure 5. Raman spectrum of (a) Raw coconut shell, (b) N-doped activated carbon material showing the D and G bands.

The ID/IG ratio provides information about the crystallite dimension, plane defects, edge defects, and the nature of disorder of the carbon derivative [37]. It is well-known that the addition of heteroatoms in the graphitic carbon lattice structure results in more defects and a larger D-band intensity [38].

To gain insight into the purity of activated carbon material, thermogravimetry coupled to mass spectrometry studies (TGA-MS) was performed, and the corresponding thermogram is presented in Figure 6. The curve is composed of two main stages with mass losses. According to mass spectrometry data, the first stage with the weaker mass loss below 100˚C can be attributed to the loss of water molecules adsorbed on the surface of the activated carbon, while a significant loss of CO_2 after 600˚C - 650˚C and carbon monoxide (CO) after 700˚C is also observed.

Figure 7 shows the FTIR pattern with functional groups of the samples. The FTIR characterization used transmittance spectrum data and was recorded between 750 - 4000 cm^{-1}. The characterization results show that a functional group on the sample surface was close to each other. The peak at approximately 3400 cm^{-1} is due to O-H vibrations, indicating the phenolic groups [39] [40] [41]. The peak at 2350 cm^{-1} and 1550 cm^{-1} corresponds to carboxylic acid with a stretching vibration of C-O [42] [43]. And the peak at 1120 cm^{-1} can be attributed to C-O [44] [45]. The functional groups of activated carbon, comprising O-H, C-O, and C-O stretching vibration, have the essential role as an absorbent of pollutant [46]. Furthermore, the functional groups containing oxygen on the sample surface are a depositional location to absorb the metal particle for catalyst application [44]. The functional groups observed in our coconut shell-based activated carbon are similar to previous research and commercial activated carbon [46].

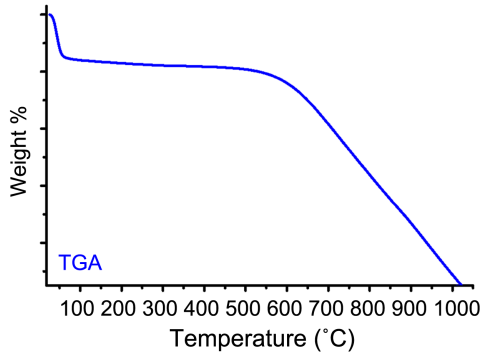

Figure 6. TGA thermogram of N-doped activated carbon.

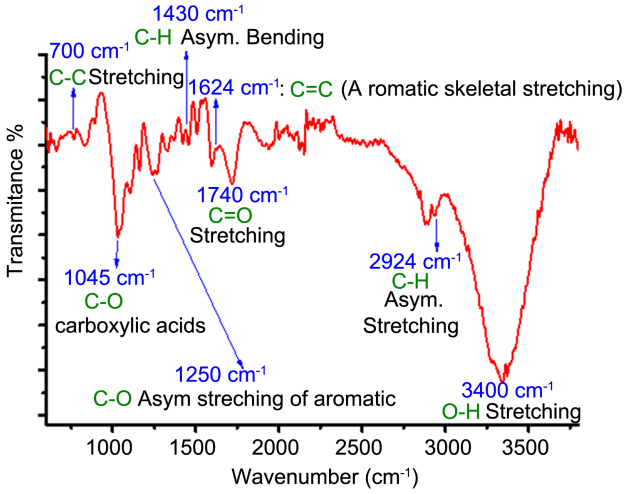

Figure 7. FTIR spectrum of N-doped activated Carbon.

3.2. Evaluation of Electrocatalytic Activity for ORR and OER

We compared the performance of our sample for ORR and OER catalyses in alkaline medium (0.1 M KOH) saturated in O_2 using LSV as shown in **Figure 8**. It is also common to perform the two reactions in the same vessel with the aim of seeking a good catalyst for regenerative fuel cell [47] [48] [49]. Comparisons of LSV data for raw coconut sample and N-doped activated carbon sample revealed that the presence of nitrogen can enhance the electrocatalytic performance, *i.e.*, higher current density and more positive onset potential (**Figure 8(A)**). The results indicate that the intercalation of nitrogen in the carbon structure can improve electrocatalytic activities for the two reactions.

To obtain insight into the number of electrons involved in the reaction, which is an important factor for fuel cell applications, Koutecky-Levich plots were used. The corresponding Koutecky-Levich plots (j^{-1} vs. (angular rotation speed, ω)$^{-1/2}$) at various electrode potentials show good linearity for N-doped activated carbon (**Figure 8(B)**); linearity and parallelism of both plots are considered as typical first-order reaction kinetics with respect to the concentration of dissolved O_2. The kinetic parameters can be analysed based on the Koutecky-Levich equations [47]:

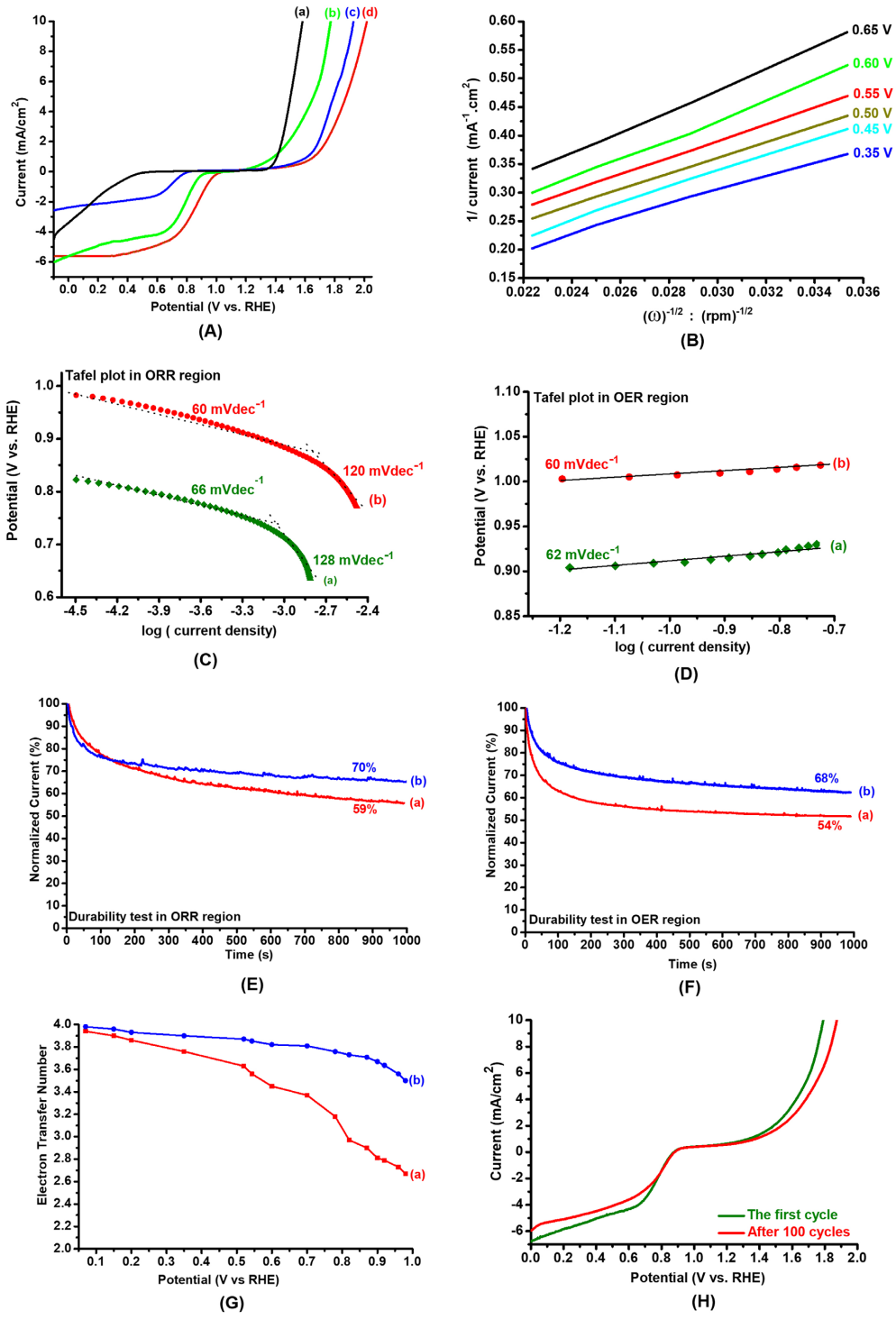

Figure 8. ORR and OER activities: (A) LSV comparison among (a) Ruthenium/C (Ru-20 wt %), (b) N-doped activated carbon, (c) raw coconut shells & (d) Pt/C (Pt-20 wt%). (B) Koutecky-Levich plots at different electrode potentials related to ORR region. (C) Tafel slope of (a) N-doped activated carbon in ORR region and (b) Pt/C 20 wt% in ORR region. (D) Tafel slope of (a) N-doped activated carbon in OER region and (b) Pt/C 20 wt% in OER region. (E) Durability/stability Test: Current-time chronoamperometric responses of (a) N-doped activated carbon and (b) Pt/C 20wt% on a GC electrode in ORR region and (F) in OER region performed in O_2-saturated 0.1 M KOH. The percentages are the reference to the initial current at time zero. (G) Calculated electron transfer number for (a) Raw coconut shells and (b) N-doped activated carbon. (H) Reversibility Test: LSV of forward current and backward current of N-doped activated carbon in O_2-0.1 M KOH at 1600 rpm, scan rate of 10 mV/s.

$$\frac{1}{j}=\frac{1}{j_L}+\frac{1}{j_K}=\frac{1}{B\omega^{1/2}}+\frac{1}{j_K}$$

$$B=0.201nFC_0\left(D_0\right)^{2/3}\nu^{-1/6}$$

$$J_K=\alpha nFC_0$$

Here, j is the measured current density; j_K and j_L are the kinetic and diffusion-limiting current densities, respectively; ω is the angular rotation speed of the disk (rpm); n is the overall number of electrons transferred in oxygen reduction; F is the Faraday constant (F = 96,485 C·mol^{-1}); C_0 is the bulk concentration of O_2; ν is the kinematic viscosity of the electrolyte; and α is the transfer coefficient. The curve j^{-1} vs. $\omega^{-1/2}$ is a straight line characterized by slope $(nB)^{-1}$ and intercept (j_K^{-1}). The slope of the straight line enables the extraction of the total number of exchanged electrons n and the intercept at the origin gives the inverse of the kinetic current j_K by using parameters C_0 = 1.2 × 10^{-3} mol·L^{-1}, D_0 =1.9 × 10^{-5} cm·s^{-1}, and ν = 0.1 m^2·s^{-1} in 0.1 M KOH. ORR can occur either *via* a direct 4-electron reduction pathway where O_2 is reduced to H_2O, a 2-electron reduction pathway where it is reduced to hydrogen peroxide (H_2O_2), or an indirect 4-electron reduction pathway where the generated H_2O_2 is further reduced to H_2O. The number of electrons transferred for N-doped activated carbon is approximately 4 while that for raw coconut is around 2 (**Figure 8(G)**). Thus, our N-doped sample shows better activity towards ORR compared to the raw sample, forming about 4 electrons during ORR, which agrees with previous papers [50] [51] [52] [53]. In this regard, Yang *et al.* [54] showed that the presence of quaternary N (graphitic N, N-bonded to three carbon atoms) atoms which have relatively low energetic barrier for donating electrons from the surface of the catalyst can also be responsible for ORR. The quaternary N atoms in graphene-typed structure could give electrons to the π-conjugated system so that it can increase nucleophile strength of the adjacent carbon rings [C(δ^-)] and improve O_2 adsorption. Since O_2 has high densities of O lone pair electrons [O(δ^-)], the presence of [C(δ^-)] can enhance ORR [55] [56]. The role of the real "electrocatalytically active sites" still remains in debate since their contribution to the catalytic activity is not well defined [57]. In some studies, the enhanced electrocatalytic activity is attributed to pyridinic-N and/or pyrrolic-N [32] [33] [58]. Miyata suggested that graphitic nitrogen is more important for the electrocatalytic activity of nitrogen-doped carbon [59]. In parallel to this data, our XPS results indicate that N-graphene also exists in the N-doped activated carbon sample. It is believed that carbon atoms adjacent to nitrogen dopants possess a substantially higher positive charge density to counterbalance the strong electronic affinity of the nitrogen atom [60], which results in an enhanced adsorption of O_2 and reactive intermediates (*i.e.*, superoxide, hydroperoxide) that proceeds to accelerate the ORR [61] [62]. The nitrogen-induced charge delocalization could also change the chemisorption mode of O_2—from monoatomic end-on adsorption on undoped carbon to a diatomic side-on adsorption at nitrogen functionalized carbon structure which effectively weakens the O-O bond to facilitate ORR [60]. This is also true for H_2O_2 reduction because breaking the

O-O bond is also a key step for the electrocatalytic reduction of H_2O_2. In addition, the presence of nitrogen in the structure enhances the ability of graphene sheets to donate electrons [33], which is advantageous for reduction reactions.

Yang *et al.* showed that the adsorption of OOH* and O* intermediates on carbon atoms next to the pyridinic N is responsible for OER [54]. Pyridinic N (an electron-withdrawing group with the lone pair electrons involved in the resonance to delocalize electrons to make the N atoms electron-deficient) can accept electrons from adjacent C atoms [C(δ^+)], facilitating the adsorption of water oxidation intermediates (OH^-, OOH^-) from catalyst surface [63] [64]. Owing to the fact that Pt is not a good catalyst for OER, we also compared the performance of our samples with Ru catalysts, which are well-known precious metal catalysts for OER. The OER activities of our sample are comparable to those of precious metal catalysts (**Figure 8(A)**).

The Tafel equation describes the electrochemical kinetics relating the rate of an electrochemical reaction to the overpotential [65]. The Tafel slope provides insight into the reaction mechanism. Larger Tafel slope indicates that a larger resistance (or a large loss of potential) is necessary to accelerate a chemical reaction. Pt/C 20 wt% exhibits Tafel slopes of 60 and 120 $mV \cdot dec^{-1}$ at high and low potentials, respectively. Tafel slopes for our sample in ORR and OER regions as shown in **Figure 8(C)** and **Figure 8(D)** demonstrate similar results as compared to Pt/C 20 wt%.

The durability/stability of the obtained sample as ORR-OER catalyst was evaluated against Pt/C electrode **Figure 8(E)** and **Figure 8(F)**; the test was performed using chronoamperometry in 0.1 M KOH solution saturated with O_2. The corresponding current-time chronoamperometric response of N-doped activated carbon exhibits a very slow attenuation with only low decay for ORR and OER regions over 1000 s. In comparison, Pt/C 20 wt% showed higher decay for ORR and OER regions. This demonstrated that the durability/stability of our catalyst is better than that of Pt catalyst. To confirm the reversibility of the catalysts, LSVs were measured using forward and backward currents as illustrated in **Figure 8(H)**. Observation of the same LSV futures of running forward and reverse currents reveals that the sample has a good reversibility for both reactions. This result reveals that performing the electrochemical measurement *via* starting from ORR region or OER region has no effect on the catalytic performance. Consequently, this catalyst can be used for regenerative fuel cell.

3.3. Comparing Oxygen Electrode Activities (OEA)

To understand the catalytic performance, we further compared the oxygen electrode activity (OEA) of our sample with the Ru and Pt commercial catalysts. Here OEA is calculated as the difference between the ORR at $-3\ mA \cdot cm^{-2}$ and OER at $10\ mA \cdot cm^{-2}$, which is the common value used in literature [49] [66]. A current density of $10\ mA \cdot cm^{-2}$ is the conventionally used in OER literature [3] [67]. Smaller OEA value indicates that the performance is closer to the ideal reversible oxygen electrode. **Table 1** shows the accumulated OEA data for all the

Table 1. Comparisons of oxygen electrode activity.

Catalyst	ORR: E(V) at I = −3 mA·cm^{-2}	OER: E(V) at I = 10 mA·cm^{-2}	Oxygen electrode activity (OEA) (OER-ORR): E(V) vs RHE
Raw Coonut Shells	-0.21	1.92	2.13
N-doped Activated Carbon	0.74	1.77	1.03
Pt/C 20 wt% (Commercial)	0.83	2.01	1.18
Ru/C 20 wt% (Commercial)	0.47	1.59	1.12

materials used in this study. To assess the overall oxygen electrode activity, the difference between the ORR and the OER metrics was considered. The OEA of N-doped activated carbon is favorably comparable to the precious metal catalysts. The presence of electron donating quaternary nitrogen atoms is favorable for ORR region. In addition, high contents of electron-withdrawing functional groups (pyridinic N, C=O) are attractive for OER, [68]. Comparison between N-doped activated carbon and the raw coconut shells indicates that the observed electrocatalytic performance is attributed to the incorporation of nitrogen groups in the sample [60] [69] [70]. The results demonstrate the low-cost and scalable synthesis for producing efficient noble-metal-free, carbon-based oxygen catalysts for a variety of electrochemical applications.

4. Conclusion

We developed a new method for synthesizing N-doped activated carbon through a catalytic process from coconut shells by annealing coconut shells at a temperature of 550˚C, then treating them with urea which yielded nitrogen-doped carbon nanostructure, and subsequent pyrolysis at 900˚C. The obtained data from the experimental measurements showed that N-doped activated carbon possesses good bifunctional electrocatalytic activities towards ORR and OER comparable with commercial catalysts including excellent stability in alkaline electrolytes. The synthesis method of using environmentally friendly coconut shells and the enhanced electrocatalytic performance of the catalyst after treatment with urea has the potential for cost-effective and mass production of efficient bifunctional green catalyst for regenerative fuel cells and other applications.

Acknowledgements

The work was funded in part by the Army Research Office (ARO) (Award No W911NF-15-1-0483) & National Science Foundation (NSF) CREST project (Award No HRD 1736136) in the USA. Also, we gratefully thank Professor Guanglin Zhao, Professor Patrick Mensah, and Dr. Rachel Vincent-Finley for their support during this project.

Conflicts of Interest

The authors declare no conflicts of interest regarding the publication of this paper.

References

[1] Ji, X., Lee, K.T., Holden, H., Zhang, L., Zhang, J., Botton, G.A., Couillard, M. and Nazar, L.F. (2010) Nanocrystalline Intermetallics on Mesoporous Carbon for Direct Formic Acid Fuel Cell Anodes. *Nature Chemistry*, **2**, 286-293. https://doi.org/10.1038/nchem.553

[2] Gray, H.B. (2009) Powering the Planet with Solar Fuel. *Nature Chemistry*, **1**, 7. https://doi.org/10.1038/nchem.141

[3] Kanan, M.W. and Nocera, D.G. (2008) *In Situ* Formation of an Oxygen-Evolving Catalyst in Neutral Water Containing Phosphate and Co^{2+}. *Science*, **321**, 1072-1075. https://doi.org/10.1126/science.1162018

[4] Lu, Y.C., Xu, Z., Gasteiger, H.A., Chen, S., Hamad-Schifferli, K. and Shao-Horn, Y. (2010) Platinum-Gold Nanoparticles: A Highly Active Bifunctional Electrocatalyst for Rechargeable Lithium-Air Batteries. *Journal of the American Chemical Society*, **132**, 12170-12171. https://doi.org/10.1021/ja1036572

[5] Suntivich, J., May, K.J., Gasteiger, H.A., Goodenough, J.B. and Shao-Horn, Y. (2011) A Perovskite Oxide Optimized for Oxygen Evolution Catalysis from Molecular Orbital Principles, *Science*, **334**, 1383-1385. https://doi.org/10.1126/science.1212858

[6] Gasteiger, H.A., Kocha, S.S., Sompalli, B. and Wagner, F.T. (2005) Activity Benchmarks and Requirements for Pt, Pt-Alloy, and Non-Pt Oxygen Reduction Catalysts for PEMFCs. *Applied Catalysis B*: *Environmental*, **56**, 9-35. https://doi.org/10.1016/j.apcatb.2004.06.021

[7] Ahn, J. and Holze, R. (1992) Bifunctional Electrodes for an Integrated Water-Electrolysis and Hydrogen-Oxygen Fuel Cell with a Solid Polymer Electrolyte. *Journal of Applied Electrochemistry*, **22**, 1167-1174. https://doi.org/10.1007/BF01297419

[8] Long, C., Qi, D., Wei, T., Yan, J., Jiang, L. and Fan, Z. (2014) Nitrogen-Doped Carbon Networks for High Energy Density Supercapacitors Derived from Polyaniline Coated Bacterial Cellulose. *Advanced Functional Materials*, **24**, 3953-3961. https://doi.org/10.1002/adfm.201304269

[9] Chen, L.F., Huang, Z.H., Liang, H.W., Gao, H.L. and Yu, S.H. (2014) Three-Dimensional Heteroatom-Doped Carbon Nanofiber Networks Derived from Bacterial Cellulose for Supercapacitors. *Advanced Functional Materials*, **24**, 5104-5111. https://doi.org/10.1002/adfm.201400590

[10] Liu, Q., Chen, C., Pan, F. and Zhang, J. (2015) Highly Efficient Oxygen Reduction on Porous Nitrogen-Doped Nanocarbons Directly Synthesized from Cellulose Nanocrystals and Urea. *Electrochimica Acta*, **170**, 234-241. https://doi.org/10.1016/j.electacta.2015.04.094

[11] Alatalo, S.M., Qiu, K., Preuss, K., Marinovic, A., Sevilla, M., Sillanpää, M., Guo, X. and Titirici, M.M. (2016) Soy Protein Directed Hydrothermal Synthesis of Porous Carbon Aerogels for Electrocatalytic Oxygen Reduction. *Carbon*, **96**, 622-630. https://doi.org/10.1016/j.carbon.2015.09.108

[12] Nguyen, T.D., Shopsowitz, K.E. and MacLachlan, M.J. (2014) Mesoporous Nitrogen-Doped Carbon from Nanocrystalline Chitin Assemblies. *Journal of Materials*

Chemistry A, **2**, 5915-5921. https://doi.org/10.1039/c3ta15255c

[13] Yuan, H., Deng, L., Cai, X., Zhou, S., Chen, Y. and Yuan, Y. (2015) Nitrogen-Doped Carbon Sheets Derived from Chitin as Non-Metal Bifunctional Electrocatalysts for Oxygen Reduction and Evolution. *RSC Advances*, **5**, 56121-56129. https://doi.org/10.1039/C5RA05461C

[14] Primo, A., Atienzar, P., Sanchez, E., Delgado, J.M. and García, H. (2012) From Biomass Wastes to Large-Area, High Quality N-Doped Graphene: Catalyst-Free Carbonization of Chitosan Coatings on Arbitrary Substrates. *Chemical Communications*, **48**, 9254-9256. https://doi.org/10.1039/c2cc34978g

[15] Rybarczyk, M.K., Lieder, M. and Jablonska, M. (2015) N-Doped Mesoporous Carbon Nanosheets Obtained by Pyrolysis of a Chitosan-Melamine Mixture for the Oxygen Reduction Reaction in Alkaline Media. *RSC Advances*, **5**, 44969-44977. https://doi.org/10.1039/C5RA05725F

[16] Liu, Q., Duan, Y., Zhao, Q., Pan, F., Zhang, B. and Zhang, J. (2014) Direct Synthesis of Nitrogen-Doped Carbon Nanosheets with High Surface Area and Excellent Oxygen Reduction Performance. *Langmuir*, **30**, 8238-8245. https://doi.org/10.1021/la404995y

[17] Yang, Y., Deng, Y., Tong, Z. and Wang, C. (2014) Renewable Lignin-Based Xerogels with Self-Cleaning Properties and Superhydrophobicity. *ACS Sustainable Chemistry & Engineering*, **2**, 1729-1733. https://doi.org/10.1021/sc500250b

[18] Liu, X., Zhou, Y., Zhou, W., Li, L., Huang, S. and Chen, S. (2015) Biomass-Derived Nitrogen Self-Doped Porous Carbon as Effective Metal-Free Catalysts for Oxygen Reduction Reaction. *Nanoscale*, **7**, 6136-6142. https://doi.org/10.1039/C5NR00013K

[19] Chen, P., Wang, L.K., Wang, G., Gao, M.R., Ge, J., Yuan, W.J., Shen, Y.H., Xie, A.J. and Yu, S.H. (2014) Nitrogen-Doped Nanoporous Carbon Nanosheets Derived from Plant Biomass: An Efficient Catalyst for Oxygen Reduction Reaction. *Energy & Environmental Science*, **7**, 4095-4103. https://doi.org/10.1039/C4EE02531H

[20] Pan, F., Cao, Z., Zhao, Q., Liang, H. and Zhang, J. (2014) Nitrogen-Doped Porous Carbon Nanosheets Made from Biomass as Highly Active Electrocatalyst for Oxygen Reduction Reaction. *Journal of Power Sources*, **272**, 8-15. https://doi.org/10.1016/j.jpowsour.2014.07.180

[21] Song, M.Y., Park, H.Y., Yang, D.S., Bhattacharjya, D. and Yu, J.S. (2014) Seaweed-Derived Heteroatom-Doped Highly Porous Carbon as an Electrocatalyst for the Oxygen Reduction Reaction. *ChemSusChem*, **7**, 1755-1763. https://doi.org/10.1002/cssc.201400049

[22] Yang, K., Peng, J., Srinivasakannan, C., Zhang, L. Xia, H. and Duan, X. (2010) Preparation of High Surface Area Activated Carbon from Coconut Shells Using Microwave Heating. *Bioresource Technology*, **101**, 6163-6169. https://doi.org/10.1016/j.biortech.2010.03.001

[23] Li, W., Yang, K., Peng, J., Zhang, L., Guo, S. and Xia, H. (2008) Effects of Carbonization Temperatures on Characteristics of Porosity in Coconut Shell Chars and Activated Carbons Derived from Carbonized Coconut Shell Chars. *Industrial Crops and Products*, **28**, 190-198. https://doi.org/10.1016/j.indcrop.2008.02.012

[24] Prauchner, M.J. and Rodríguez-Reinoso, F. (2012) Chemical versus Physical Activation of Coconut Shell: A Comparative Study. *Microporous and Mesoporous Materials*, **152**, 163-171. https://doi.org/10.1016/j.micromeso.2011.11.040

[25] Rout, T., Pradhan, D., Singh, R.K. and Kumari, N. (2016) Exhaustive Study of Products Obtained from Coconut Shell Pyrolysis. *Journal of Environmental Chemical Engineering*, **4**, 3696-3705. https://doi.org/10.1016/j.jece.2016.02.024

[26] Heschel, W. and Klose, E. (1995) On the Suitability of Agricultural By-Products for the Manufacture of Granular Activated Carbon. *Fuel*, **74**, 1786-1791. https://doi.org/10.1016/0016-2361(95)80009-7

[27] Sekhon, S.S., Kaur, P. and Park, J. (2021) From Coconut Shell Biomass to Oxygen Reduction Reaction Catalyst: Tuning Porosity and Nitrogen Doping. *Renewable and Sustainable Energy Reviews*, **147**, Article ID: 111173. https://doi.org/10.1016/j.rser.2021.111173

[28] Madakson, P., Yawas, D.S. and Apasi, A. (2012) Characterization of Coconut Shell Ash for Potential Utilization in Metal Matrix Composites for Automotive Applications. *International Journal of Engineering, Science and Technology*, **4**, 1190-1198.

[29] Bakti, A.I. and Gareso, P.L. (2018) Characterization of Active Carbon Prepared from Coconuts Shells Using FTIR, XRD and SEM Techniques. *Jurnal ilmiah pendidikan fisika Al-Biruni*, **7**, 33-39. https://doi.org/10.24042/jipfalbiruni.v7i1.2459

[30] Yang, M., Guo, L., Hu, G., Hu, X., Xu, L., Chen, J., Dai, W. and Fan, M. (2015) Highly Cost-Effective Nitrogen-Doped Porous Coconut Shell-Based CO_2 Sorbent Synthesized by Combining Ammoxidation with KOH Activation. *Environmental Science & Technology*, **49**, 7063-7070. https://doi.org/10.1021/acs.est.5b01311

[31] Shao,Y., Zhang, S., Engelhard, M.H., Li, G., Shao, G., Wang, Y., Liu, J., Aksay, I.A. and Lin, Y. (2010) Nitrogen-Doped Graphene and Its Electrochemical Applications. *Journal of Materials Chemistry*, **20**, 7491-7496. https://doi.org/10.1039/c0jm00782j

[32] Matter, P.H., Zhang, L. and Ozkan, U.S. (2006) The Role of Nanostructure in Nitrogen-Containing Carbon Catalysts for the Oxygen Reduction Reaction. *Journal of Catalysis*, **239**, 83-96. https://doi.org/10.1016/j.jcat.2006.01.022

[33] Kundu, S., Nagaiah, T.C., Xia, W., Wang, Y., Dommele, S.V., Bitter, J.H., Santa, M., Grundmeier, G., Bron, M. and Schuhmann, W. (2009) Electrocatalytic Activity and Stability of Nitrogen-Containing Carbon Nanotubes in the Oxygen Reduction Reaction. *The Journal of Physical Chemistry C*, **113**, 14302-14310. https://doi.org/10.1021/jp811320d

[34] Arrigo, R., Hävecker, M., Schlögl, R. and Su, D.S. (2008) Dynamic Surface Rearrangement and Thermal Stability of Nitrogen Functional Groups on Carbon Nanotubes. *ChemComm*, **40**, 4891-4893. https://doi.org/10.1039/b812769g

[35] Sadezky, A., Muckenhuber, H., Grothe, H., Niessner, R. and Poschl, U. (2005) Raman Micro Spectroscopy of Soot and Related Carbonaceous Materials: Spectral Analysis and Structural Information. *Carbon*, **43**, 1731-1742. https://doi.org/10.1016/j.carbon.2005.02.018

[36] Fahmi, F., Dewayanti, N.A.A., Widiyastuti, W. and Setyawan, H. (2020) Preparation of Porous Graphene-Like Material from Coconut Shell Charcoals for Supercapacitors. *Cogent Engineering*, **7**, Article ID: 1748962. https://doi.org/10.1080/23311916.2020.1748962

[37] Kumar, M.P., Kesavan, T., Kalita, G., Ragupathy, P., Narayanan, T.N. and Pattanayak, D.K. (2014) On the Large Capacitance of Nitrogen Doped Graphene Derived by a Facile Route. *RSC Advances*, **4**, 38689-38697. https://doi.org/10.1039/C4RA04927F

[38] Sharifi, T., Nitze, F., Barzegar, H.R., Tai, W.C., Mazurkiewicz, M., Malolepszy, A., Stobinski, L. and Wagberg, T. (2012) Nitrogen Doped Multi Walled Carbon Nanotubes Produced by CVD-Correlating XPS and Raman Spectroscopy for the Study of Nitrogen Inclusion. *Carbon*, **50**, 3535-3541. https://doi.org/10.1016/j.carbon.2012.03.022

[39] Valencia, A., Muniz-Valencia, R., Ceballos-Magana, S.G., Rojas-Mayorga, C.K., Bo-

nilla-Petriciolet, A., Gonz'alez, J. and Aguayo-Villarreal, I.A. (2022) Cyclohexane and Benzene Separation by Fixed-Bed Adsorption on Activated Carbons Prepared from Coconut Shell. *Environmental Technology & Innovation*, **25**, Article ID: 102076. https://doi.org/10.1016/j.carbon.2012.03.022

[40] Huang, Y., Ma, E. and Zhao, G. (2015) Thermal and Structure Analysis on Reaction Mechanisms during the Preparation of Activated Carbon Fibers by KOH Activation from Liquefied Wood-Based Fibers. *Industrial Crops and Products*, **69**, 447-455. https://doi.org/10.1016/j.indcrop.2015.03.002

[41] Rawal, S., Joshi, B. and Kumar, Y. (2018) Synthesis and Characterization of Activated Carbon from the Biomass of *Saccharum bengalense* for Electrochemical Supercapacitors. *Journal of Energy Storage*, **20**, 418-426. https://doi.org/10.1016/j.est.2018.10.009

[42] Freitas, J.V., Nogueira, F.G.E. and Farinas, C.S. (2019) Coconut Shell Activated Carbon as an Alternative Adsorbent of Inhibitors from Lignocellulosic Biomass Pretreatment. *Industrial Crops and Products*, **137**, 16-23. https://doi.org/10.1016/j.indcrop.2019.05.018

[43] Pallar'es, J., Gonzalez-Cencerrado, A. and Arauzo, I. (2018) Production and Characterization of Activated Carbon from Barley Straw by Physical Activation with Carbon Dioxide and Steam. *Biomass Bioenergy*, **115**, 64-73. https://doi.org/10.1016/j.biombioe.2018.04.015

[44] Li, X., Wang, Y., Zhang, G., Sun, W., Bai, Y., Zheng, L., Han, X. and Wu, L. (2019) Influence of Mg-Promoted Ni-Based Catalyst Supported on Coconut Shell Carbon for CO_2 Methanation. *Chemistry Select*, **4**, 838-845. https://doi.org/10.1002/slct.201803369

[45] Saleh, T.A. (2018) Simultaneous Adsorptive Desulfurization of Diesel Fuel over Bimetallic Nanoparticles Loaded on Activated Carbon. *Journal of Cleaner Production*, **172**, 2123-2132. https://doi.org/10.1016/j.jclepro.2017.11.208

[46] Shu, J., Cheng, S., Xia, H., Zhang, L., Peng, J., Li, C. and Zhang, S. (2017) Copper Loaded on Activated Carbon as an Efficient Adsorbent for Removal of Methylene Blue. *RSC Advances*, **7**, 14395-14405. https://doi.org/10.1039/C7RA00287D

[47] Jahan, M., Tominaka, S. and Henzie, J. (2016) Phase Pure α-Mn_2O_3 Prisms and Their Bifunctional Electrocatalytic Activity in Oxygen Evolution and Reduction Reactions. *Dalton Transactions*, **45**, 18494-18501. https://doi.org/10.1039/C6DT03158G

[48] Gorlin, Y., Lassalle-Kaiser, B., Benck, J.D., Gul, S., Webb, S.M., Yachandra, V.K., Yano, J. and Jaramillo, T.F. (2013) n Situ X-Ray Absorption Spectroscopy Investigation of a Bifunctional Manganese Oxide Catalyst with High Activity for Electrochemical Water Oxidation and Oxygen Reduction. *Journal of the American Chemical Society*, **135**, 8525-8534. https://doi.org/10.1021/ja3104632

[49] Gorlin, Y. and Jaramillo, T.F. (2010) A Bifunctional Nonprecious Metal Catalyst for Oxygen Reduction and Water Oxidation. *Journal of the American Chemical Society*, **132**, 13612-13614. https://doi.org/10.1021/ja104587v

[50] Li, J., Liu, G., Liu, B., Min, Z., Qian, D., Jiang, J. and Li, J. (2018) Fe-Doped $CoSe_2$ Nanoparticles Encapsulated in N-Doped Bamboo-Like Carbon Nanotubes as an Efficient Electrocatalyst for Oxygen Evolution Reaction. *Electrochimica Acta*, **265**, 577-585. https://doi.org/10.1016/j.electacta.2018.01.211

[51] Yang, W., Liu, X., Yue, X., Jia, J. and Guo, S. (2015) Bamboo-Like Carbon Nanotube/Fe_3C Nanoparticle Hybrids and Their Highly Efficient Catalysis for Oxygen Reduction. *Journal of the American Chemical Society*, **137**, 1436-1439.

https://doi.org/10.1021/ja5129132

[52] Li, J., Chen, J., Wang, H., Ren, Y., Liu, K., Tang, Y. and Shao, M. (2017) Fe/N Co-Doped Carbon Materials with Controllable Structure as Highly Efficient Electrocatalysts for Oxygen Reduction Reaction in Al-Air Batteries. *Energy Storage Mater.* **8**, 49-58. https://doi.org/10.1016/j.ensm.2017.03.007

[53] Li, Z., Sun, H., Wei, L., Jiang, W.J., Wu, M. and Hu, J.S. (2017) Lamellar Metal Organic Framework-Derived Fe-N-C Non-Noble Electrocatalysts with Bimodal Porosity for Efficient Oxygen Reduction. *ACS Applied Materials & Interfaces*, **9**, 5272-5278. https://doi.org/10.1021/acsami.6b15154

[54] Yang, H.B., Miao, J., Hung, S.F., Chen, J., Tao, H.B., Wang, X., Zhang, L., Chen, R., Gao, J. and Chen, H.M. (2016) Identification of Catalytic Sites for Oxygen Reduction and Oxygen Evolution in N-Doped Graphene Materials: Development of Highly Efficient Metal-Free Bifunctional Electrocatalyst. *Science Advances*, **2**, e1501122. https://doi.org/10.1126/sciadv.1501122

[55] Luo, Z., Lim, S., Tian, Z., Shang, J., Lai, L., MacDonald, B., Fu, C., Shen, Z., Yu, T. and Lin, J. (2011) Pyridinic N Doped Graphene: Synthesis, Electronic Structure, and Electrocatalytic Property. *Journal of Materials Chemistry*, **21**, 8038-8044. https://doi.org/10.1039/c1jm10845j

[56] Okamoto, Y. (2009) First-Principles Molecular Dynamics Simulation of O_2 Reduction on Nitrogen-Doped Carbon. *Applied Surface Science*, **256**, 335-341. https://doi.org/10.1016/j.apsusc.2009.08.027

[57] Shao, Y., Sui, J., Yin, G. and Gao, Y. (2008) Nitrogen-Doped Carbon Nanostructures and Their Composites as Catalytic Materials for Proton Exchange Membrane Fuel Cell. *Applied Catalysis B*, **79**, 89-99. https://doi.org/10.1016/j.apcatb.2007.09.047

[58] Arrigo, R., Hävecker, M., Schlögl, R. and Su, D.S. (2008) Dynamic Surface Rearrangement and Thermal Stability of Nitrogen Functional Groups on Carbon Nanotubes. *Chemical Communications*, **40**, 4891-4893. https://doi.org/10.1039/b812769g

[59] Niwa, H., Horiba, K., Harada, Y., Oshima, M., Ikeda, T., Terakura, K., Ozaki, J. and Miyata, S. (2009) X-Ray Absorption Analysis of Nitrogen Contribution to Oxygen Reduction Reaction in Carbon Alloy Cathode Catalysts for Polymer Electrolyte Fuel Cells. *Journal of Power Sources*, **187**, 93-97. https://doi.org/10.1016/j.jpowsour.2008.10.064

[60] Gong, K., Du, F., Xia, Z., Durstock, M. and Dai, L. (2009) Nitrogen-Doped Carbon Nanotube Arrays with High Electrocatalytic Activity for Oxygen Reduction. *Science*, **323**, 760-764. https://doi.org/10.1126/science.1168049

[61] Maldonado, S. and Stevenson, K.J. (2005) Influence of Nitrogen Doping on Oxygen Reduction Electrocatalysis at Carbon Nanofiber Electrodes. *The Journal of Physical Chemistry B*, **109**, 4707-4716. https://doi.org/10.1021/jp044442z

[62] Gao, F., Zhao, G.L. and Yang, S. (2014) Catalytic Reactions on the Open-Edge Sites of Nitrogen-Doped Carbon Nanotubes as Cathode Catalyst for Hydrogen Fuel Cells. *ACS Catalysis*, **4**, 1267-1273. https://doi.org/10.1021/cs500221m

[63] Man, I.C., Su, H.Y., Calle‐Vallejo, F., Hansen, H.A., Martínez, J.I., Inoglu, N.G., Kitchin, J., Jaramillo, T.F., Nørskov, J.K. and Rossmeisl, J. (2011) Universality in Oxygen Evolution Electrocatalysis on Oxide Surfaces. *ChemCatChem*, **3**, 1159-1165. https://doi.org/10.1002/cctc.201000397

[64] Dau, H., Limberg, C., Reier, T., Risch, M., Roggan, S. and Strasser, P. (2010) The Mechanism of Water Oxidation: From Electrolysis via Homogeneous to Biological Catalysis. *ChemCatChem*, **2**, 724-761. https://doi.org/10.1002/cctc.201000126

[65] Lim, S., Yoon, S.H., Mochida, I. and Jung, D.H. (2009) Direct Synthesis and Structural Analysis of Nitrogen-Doped Carbon Nanofibers. *Langmuir*, **25**, 8268-8273. https://doi.org/10.1021/la900472d

[66] Jiang, H., Yao, Y., Zhu, Y., Liu, Y., Su, Y., Yang, X. and Li, C. (2015) Iron Carbide Nanoparticles Encapsulated in Mesoporous Fe-N-Doped Graphene-Like Carbon Hybrids as Efficient Bifunctional Oxygen Electrocatalysts. *ACS Applied Materials & Interfaces*, **7**, 21511-21520. https://doi.org/10.1021/acsami.5b06708

[67] Lewis, N.S. and Nocera, D.G. (2006) Powering the Planet: Chemical Challenges in Solar Energy Utilization. *PANS*, **103**, 15729-15735. https://doi.org/10.1073/pnas.0603395103

[68] He, W., Xue, P., Du, H., Xu, L., Pang, M., Gao, X., Yu, J., Zhang, Z. and Huang, T. (2017) A Facile Method Prepared Nitrogen and Boron Doped Carbon Nano-Tube Based Catalysts for Oxygen Reduction. *International Journal of Hydrogen Energy*, **42**, 4123-4132. https://doi.org/10.1016/j.ijhydene.2017.01.134

[69] Yang, J., Liu, D.J., Kariuki, N.N. and Chen, L.X. (2008) Aligned Carbon Nanotubes with Built-In FeN_4 Active Sites for Electrocatalytic Reduction of Oxygen. *Chemical Communications*, **3**, 329-331. https://doi.org/10.1039/B713096A

[70] Wu, G., More, K.L., Johnston, C.M. and Zelenay, P. (2011) High-Performance Electrocatalysts for Oxygen Reduction Derived from Polyaniline, Iron, and Cobalt. *Science*, **332**, 443-447. https://doi.org/10.1126/science.1200832